Scaling Law Analysis of Electrohydrodynamics and Dielectrophoresis for Isomotive Dielectrophoresis Microfluidic Devices

Journal:	*ELECTROPHORESIS*
Manuscript ID	elps.201900311.R1
Wiley - Manuscript type:	Research Paper
Date Submitted by the Author:	09-Oct-2019
Complete List of Authors:	Rashed, Mohamed; University of Louisville , Electrical & Computer Engineering Green, Nicolas; University of Southampton, School of Electronics and Computer Science Williams, Stuart; University of Louisville, Mechanical Engineering
Keywords:	Isomotive dielectrophoresis, Dielectrophoresis, Electrothermal hydrodynamics, Electrothermal flow, Joule heating

SCHOLARONE™
Manuscripts

Scaling Law Analysis of Electrohydrodynamics and Dielectrophoresis for Isomotive Dielectrophoresis Microfluidic Devices

Mohamed Z. Rashed, Nicolas G. Green, and Stuart J. Williams*

Mohamed Z Rashed

University of Louisville, Sacket Hall 200,

Louisville, 40292 KY, USA

mohamed.rashed@louisville.edu; https://orcid.org/0000-0001-8464-5727

+1 (502) 309-8117

Nicolas G. Green

Electronics and Computer Science,

University of Southampton Highfield Campus,

Highfield, SO17 1BJ, Southampton, United Kingdom

ng2@ecs.soton.ac.uk; https://orcid.org/0000-0001-9230-4455

*Stuart J. Williams

University of Louisville, Sacket Hall 200,

Louisville, 40292 KY

USA

stuart.williams@louisville.edu; https://orcid.org/0000-0002-1678-7544

For Peer Review

+1 (502) 852 6340

Abbreviations

ACEO: AC electro-osmosis

CM: Clausius Mossotti

DEP: dielectrophoresis

DRIE: Deep Reactive Ion Etching

ET: Electro Thermal

isoDEP: Isomotive dielectrophoresis

nDEP: negative dielectrophoresis

pDEP: positive dielectrophoresis

Keywords

Dielectrophoresis, Electrothermal flow, Electrothermal hydrodynamics, Isomotive dielectrophoresis, Joule heating

For Peer Review

Abstract

Isomotive dielectrophoresis (isoDEP) is a unique dielectrophoresis (DEP) geometrical configuration where the gradient of the field-squared ($\nabla E_{\mathrm{rms}}^2$) is constant. IsoDEP analyzes polarizable particles based on their magnitude and direction of translation. Particle translation is a function of the polarizability of both the particles and suspending medium, the particles' size and shape, and the frequency of the electric field. However, other electrokinetics act on the particles simultaneously, including electrothermal hydrodynamics. Hence, to maximize the DEP force relative to over electrokinetic forces, design parameters such as microchannel geometry, fabrication materials, and applied electric field must be properly tuned. In this work, scaling law analyses were developed to derive design rules, relative to particle diameter, to reduce unwanted electrothermal hydrodynamics relative to DEP-induced particle translation. For a particle suspended in 10 mS/m media, if the channel width and height are below 10 particle diameters, the electrothermal-driven flow is reduced by ~500 times compared to a channel that is 250 particles diameters in width and height. Replacing glass with silicon as the device's underlying substrate for an insulative-based isoDEP reduces the electrothermal induced flow approximately 20 times less.

Color online: See article online to view Figs. 1–5 in color.

For Peer Review

1. Introduction

Dielectrophoresis (DEP) is the movement of polarizable particles when exposed to a non-uniform AC electric field. Non-uniform electric fields can either be generated by means of (i) insulator structures or (ii) microelectrodes [1, 2]. The dielectrophoretic response of bio-particles are a function of their dielectric properties, which is influenced by their structural, morphological, and chemical characteristics. Therefore, each bio-particle has its own dielectric signature which has been demonstrated for a variety of cells [3]. DEP has been extensively used for selective separation and concentration of bio-particles and, since DEP depends on the bio-particles' intrinsic electrical properties, electrokinetic manipulation techniques do not require any labeling. DEP has trapped, manipulated, or sorted nanoparticles [4, 5], proteins [6], DNA [7, 8], viruses [5], and enabled particle patterning [9, 10] which has paved the way to other electrokinetic patterning techniques [11].

An important feature of DEP lies in its analytical capabilities. However, straightforward analytical application of DEP is nontrivial using traditional coplanar microelectrode designs and fabrication techniques. This is because the electric field within DEP systems is inherently, and purposefully, non-uniform whose force is proportional to the gradient of the field-squared ($\nabla E_{\mathrm{rms}}^2$). In traditional DEP systems the force exerted on a particle is spatially non-uniform, typically by orders of magnitude over relatively short distances. For example, using coplanar electrodes the DEP force is greatest close to the surface of the electrodes but exponentially decreases with height above the electrode plane. Consider a 25 μm gap between two coplanar electrodes, the magnitude of the DEP force is approximately 100 times less for a particle 10 μm above the electrode edge compared to a distance of 1 μm [12]. Hence, an analytical DEP system is nontrivial because particles at different locations will be subjected to different DEP forces. To simplify analysis $\nabla E_{\mathrm{rms}}^2$ must be

For Peer Review

constant within the region of interest. Inspired by Pohl's design [13], Williams' group introduced a DEP based analytical microfluidic device named isomotive dielectrophoresis (isoDEP) using extruded two dimensional features with a specific contour [14] that produced a constant DEP force. The primary advantage of isoDEP is that the response of a particle is uniform throughout the analytical space can be obtained via particle tracking; this concept is analogous to how particle rotation is used to measure particle dielectric properties through measuring their rotational speed [15, 16]. Other designs have followed the premise of the isoDEP design and have been used successfully for single-cell analysis applications [17, 18].

In addition to DEP, the applied AC field will also induce other electrokinetic phenomena such as: (i) Joule heating [19-22]; (ii) AC electro-osmosis (ACEO) where the induced flow is generated by the action of an electric field on induced diffuse charges near a polarizable surface [23, 24]; and (iii) AC electrothermal hydrodynamics which occurs when the field interacts with fluid temperature gradients [25]. Such forces generate non-desirable fluid motion that impacts of the desired performance of isoDEP devices. Unwanted electrokinetics can be reduced through analysis of device dimensions, material properties, media properties, and the magnitude of the applied AC field. The goal of this study is to determine their impact on particle translation relative to particle translation caused by DEP forces within an isoDEP device, thereby enhancing its analytical capabilities.

IsoDEP produces a uniform DEP force using two different configurations: an electrode-based and an insulator-based arrangement In Allen et al.'s work [14], the electric field required to induce the DEP effect was approximately 68 kV/m and 50 kV/m for the electrode-based and insulator-based versions, respectively. In general, the insulative-based design might require higher applied voltages to achieve the same DEP effect. This is due to the larger distance between the electrodes

For Peer Review

(on the order of millimeters) which requires higher voltages to achieve the same field strength compared to the electrode-based design. At these large fields (> 50 kV/m) cell death may occur if cells are exposed for several minutes or at low frequencies [26-28]; however, this is not the case for isoDEP where the field is applied to an individual cell for less than a minute . In addition, high electric fields cause Joule heating which, in turn, causes the local temperature-induced variations in the conductivity (σ_m) and permittivity (ε_m) of the suspending medium causing electrothermal forces [12, 19]. Jaeger et al.[29] found that the electric field induced temperature rise is proportional to conductivity of the medium, which impacts studies with biological cells as they require suspension in conductive media (typically larger than 0.1 S/m). Although reducing the conductivity of the suspending media can mitigate Joule heating, it's not the ideal solution when considering cell viability [22]. 3D extruded electrode designs have been proposed to reduce Joule heating 8–10 times lower than planar electrode designs, because it requires lower electric fields to obtain same DEP effect along the channel's depth [30].

AC electro-osmosis (ACEO) is generated from the movement of ions in the electric double layer at the interface between electrode and media. ACEO can be prominent at lower frequencies (typically below 10 kHz) due to the frequency depenent polarization of the electrdoe double layer which disperses at higher frequencies [21]. Fortunately, ACEO can be considered negligible in isoDEP as the tangential component of the electric field at the electrode surface is significantly weaker due to the inherent geometrical configuration of isoDEP, especially compared to other microelectrode geometries like interdigitated electrodes [14, 31].

The most significant undesired electrohydrodynamic force that occurs in an isoDEP device is derived from electrothermal (ET) hydrodynamics [25, 32, 33]. Therefore, purpose of this manuscript is to develop design rules for the geometrical configuration of an isoDEP system and

For Peer Review

develop scaling laws [22] to minimize ET flow relative to isoDEP-induced particle translation for both microelectrode and insulative platforms. These design rules are based on analytical predictions, putting into account how the DEP and ET velocity scale with electrode size, applied voltage, fluid conductivity, and the size of the particles. This approach can be applied to other DEP systems that want to reduce unwanted ET flow.

2. Methods

In this section, we will be developing the electrokinetic and heat transfer equations, with some simplifying assumptions, and apply them to isoDEP device geometry. First, we will derive particle translation due to isoDEP in terms of particle diameters per second for a given device length scale and applied potential. Second, for a given particle translational velocity we determined the resultant Joule heating due to the applied field for a given device configuration and channel length scale using analytical conduction relationships based on the device geometry. Last, electrothermal hydrodynamics was estimated from calculated temperature gradients. ET motion is presented relative to isoDEP translation for a range of microchannel geometries.

IsoDEP devices have two general configurations. First is a microelectrode-based isoDEP device where the microchannel wall itself serves as the electrode; one method of fabricating this type of device is to perform DRIE of doped silicon bonded between two glass substrates [14, 17]. The second configuration is an insulative-based device where the microchannel walls are formed from electrically insulative materials (ex: SU8, PDMS, or glass [1, 34]) and the electric field is applied through the channel itself. The curvature of the isoDEP microchannel walls needs to follow the curvature illustrated in Figure 1A. The largest channel width occurs at $\theta = 60°$ and is defined as the characteristic width, r_{60} (Fig. 1A). For the insulative device L refers to the distance between the device origin and the downstream electrode (Fig. 1A) [14, 35]. The insulative isoDEP device is less

For Peer Review

expensive due to more simplistic fabrication methods (ex: soft lithography) compared to extruded microelectrode-based platforms; however, a significantly higher voltage is required from the insulative platforms for comparable DEP performance due to the longer distance between the electrodes.

Several geometric parameters were defined for the proceeding analysis. The microelectrode device (Fig. 1B) has a microchannel height h, a lid and base thickness of t_{me}, and an electrode wall thickness of t_{wall}. The insulative device (Fig. 1C) has a microchannel height h, top insulative thickness t_{ins}, and a substrate thickness t_{base}.

If the channel configuration follows that of Figure 1A the applied electric potential will yield a constant $\nabla E_{\mathrm{rms}}^2$ (refer to [14] for derivation). The potential will be in one of the following forms (in cylindrical coordinates)

$$V = {}^{2}\!/_{3}\, k\, r^{{}^{2}\!/_{3}} \sin(3\theta/2) \qquad \text{for electrode-based} \qquad (1)$$

$$V = {}^{2}\!/_{3}\, k\, r^{{}^{2}\!/_{3}} cos(3\theta/2) \qquad \text{for insulative-based} \qquad (2)$$

where $k^2 = \nabla(|E|^2) = \frac{9(\Delta V)^2}{4\ (\delta)^3}$, and δ is the characteristic electrode spacing ($\delta = r_{60}$ for microelectrode-based and $\delta = L$ for insulative-based devices), and ΔV is the potential difference between the origin and δ. The length scale guides overall electrokinetic behavior and, thus, should be selected based the performance of desired particle translation. First, the magnitude of gradient field-squared k^2will determine the field strength required to translate a particle of radius, *a,* with a velocity, $v = (2a)\, n$, expressed as an increment of n particle diameters per second. Assuming Stokes drag and that the particle has reached terminal velocity, the particle's dielectrophoretic velocity is related to n with

For Peer Review

$$\boldsymbol{v}_{\mathrm{DEP}} = \frac{\boldsymbol{F}_{\mathrm{DEP}}}{6\pi\mu a} = \frac{2\pi\varepsilon_m a^3 Re[f_{CM}](k^2)}{6\pi\mu a} = (2a)n. \quad (3)$$

These relationships were used to correlate k^2 with particle size, particle translation, device length scale, and the applied potential.

Next, the required $k^2$is found for a desired isoDEP particle translation and device geometry. Then temperature gradients were estimated from the input field strength (which is a function of k^2) and the heat transfer properties of the device. Heat conduction was assumed to be the dominant mode of heat transfer due to the nature of Joule heating being accompanied with a low Nusselt number [20, 23, 36]. The heat conduction model was used to find the temperature at the microchannel walls and the maximum temperature in the center of the channel; hence, the temperature gradient within the channel itself can be subsequently calculated.

For simplification of the heat transfer model, a rectangular channel geometry of a fixed width, w, is used. The outside wall temperature, T_{wall}, is assumed to be the same around the device perimeter (isothermal).

The heat transfer model herein combines two approaches: (i) heat transfer resistance models for calculations through the solid material and (ii) analytical estimations for the relationship of the channel wall temperature and the maximum temperature. The resistance models are illustrated in Figure 2. The lid material is attributed with a thermal resistance, R_{lid}, which is in parallel with the resistance attributed to the base material R_{base}. Resistance is related to conduction shape factor, S, with $R = \frac{1}{SK}$ where K is the material thermal conductivity. The shape factor of the lid and base assumes the microfluidic channel as an isothermal rectangular parallelepiped buried in semi-infinite medium having an isothermal surface; for this case the doncution shape factor will be [37, 38]

For Peer Review

$$S = 1.685\, L_c\left[log\left(1+\frac{t_s}{w}\right)\right]^{-0.59}(t_s/h)^{-0.078} \quad (4)$$

where L_c is microchannel length and t_s is the substrate thickness (either t_{me}, t_{base}, or t_{ins}). The electrode-based version included another resistance element that takes into account heat transfer through the conductive wall features, $R_{wall} = t_{wall}/(K\, h\, L_c)$. The equivalent resistance network, R_{eq}, is related to the heat generated inside of the microchannel, q, with $q = (T_{wall} - T_o)/R_{eq}$ where T_o is the outside ambient temperature. For simplicity, T_o is set to zero such that subsequent temperature calculations will reflect those above ambient conditions. The wall temperature can be related to device parameters from

$$T_{wall} = R_{eq}\, q = R_{eq}(\sigma_m E^2)(\delta\, h\, L_c) = R_{eq}(\sigma_m\, k^2 r)(\delta\, h\, L_c) \quad (5)$$

where σ_m is fluid conductivity, $|E|^2 = k^2 r$, and $\delta = r_{60}$ or L for an electrode-based or insulative-based device, respectively. Both insulative and electrode-based maximum temperatures are linearly proportional to r. The wall temperature will be independent of channel length, L_c, as this term in Eq. (5) will cancel with itself from R_{eq}.

The maximum temperature at the center of the microchannel at a given radial location is calculated using a 2D solution from from J.H. VanSant [39] where the temperature, T, inside of a rectangular isothermal perimeter (T_{wall}) with volumetric heating, q''', heated, is a function of its position (using Cartesian coordinates, x,y)

$$\frac{(T - T_{wall})K}{q''' {h/2}^2} = \frac{1}{2}(1 - Y^2) - 2 \times \sum_{n=0}^{\infty} \frac{(-1)^n \cosh\left[(2n+1)\frac{\pi}{2}X\right]\cos\left[(2n+1)\frac{\pi}{2}Y\right]}{\left[(2n+1)\frac{\pi}{2}\right]^3 \cosh\left[(2n+1)\frac{\pi}{2}B\right]} \quad (6a)$$

where, $Y = \frac{y}{h/2}$, $X = \frac{x}{h/2}$, $B = \frac{w}{h}$. This expression simplifies for the temperature at the center of the channel, T_{max} at $x = 0$ and $y = 0$, with

For Peer Review

$$\frac{(T_{max}-T_{wall})K}{q''' h/2^2} = \frac{1}{2} - 2 \times \sum_{n=0}^{\infty} \frac{(-1)^n}{\left[(2n+1)\frac{\pi}{2}\right]^3 \cosh\left[(2n+1)\frac{\pi}{2}B\right]} \quad (6b)$$

where volumetric heating (i.e., Joule heating) is $q''' = \sigma_m E \cdot E$.

Hence, after T_{max} is calculated, the temperature gradient can be calculated between the center of the channel and the wall (described in sections 2.1 and 2.2); only the temperature gradients along the direction of the electric field were considered for ET flow (Fig. 3) since it is proportional to $\nabla T \cdot E$ (see section 2.3).

2.1 Insulative-based device temperature gradient

The temperature gradient (∇T) along the direction of the channel is needed for the insulative-based design (Fig. 3B); this can be estimated by taking the derivative of T_{wall} in Eq. (5) with respect to the radial direction, resulting in

$$\frac{\partial T_{wall}}{\partial r} = R_{eq}(\sigma\, k^2)(L\, h\, L_c) \quad (7)$$

which includes the substitution of $\delta = L$. In insulative isoDEP device $R_{eq}$is the equivalent heat resistance of R_{lid} and R_{base} in parallel (Fig. 2B), i.e., $R_{eq} = \left(\frac{R_{base} \times R_{lid}}{R_{base} + R_{lid}}\right)$. The gradient of T_{max}, $\frac{\partial T_{max}}{\partial r}$, can be similarly calculated

The representative temperature gradient of the insulative platform, ∇T_I, is taken as the average of these

$$\nabla T_I = \frac{\partial T_{wall}}{\partial r} + \frac{1}{3}\left(\frac{\partial T_{max}}{\partial r} - \frac{\partial T_{wall}}{\partial r}\right) \quad (8)$$

Heating is proportional to radial position, $q''' = \sigma_m |E|^2 = \sigma_m\ k^2\, r$. For ET flow analysis heating will be evaluated at $r = L$. Since $\nabla T_I \cdot E$ acts in equal and opposite directions on either side of the origin (Fig 3B), the net effect will be

For Peer Review

$$\left(\nabla T_I\, E^2\right)_{net} = 2\nabla T_I\, k^2(L) sin\, 30 = \nabla T_I\, k^2\, L \quad (9)$$

2.2 Electrode-based device temperature gradient

The wall temperature for the electrode-based device is determined by substituting $\delta = r_{60}$ into Eq. (5) with $R_{eq} = \left(\frac{R_{wall} \times R_{base} \times R_{lid}}{R_{wall}\,(R_{base} + R_{lid}) + 2R_{base} \times R_{lid}}\right)$ (Fig. 2A) and choosing $r = r_{60}$. Next, T_{max} is calculated from (6b) also at $r = r_{60}$. The temperature gradient for the microelectrode system in the, ∇T_E, is calculated using with

$$\nabla T_E = (T_{max} - T_{wall}) / \left(\frac{1}{2} r_{60}\right). \quad (10)$$

Similarly, $\nabla T_E\, E^2$ was be at $r = r_{60}$ withn $E^2 = k^2\, r_{60}$ leading to

$$\nabla T_E\, E^2 = \nabla T_E\, k^2\, r_{60} \quad (11)$$

2.3 Electrothermal flow

The non-uniform electric field driving the DEP force will also act on both bound and free charges inside the suspending media which respond differently to the field, resulting in a non-zero body force on the media

$$f_{ET} = \rho_m E - \frac{1}{2}|E|^2 \nabla \varepsilon_m \quad (12)$$

where ρ_m and ε_m are the suspending media's volume charge density and the permittivity, respectively. The first and second terms on the right-hand side express the Coulomb force on the free and bound charges, respectively. The free charges relate to the conductivity of the media and represent the conduction force, while the bound charges relate to the permittivity and represent the dielectric force. Following the analysis from Castellanos et al. 2003 [22], the non-zero time-averaged electrothermal force will be

For Peer Review

$$\langle f_{\mathrm{ET}} \rangle = \frac{1}{2} Re\left(\frac{\sigma_m \varepsilon_m (\alpha - \beta)}{\sigma_m + i\omega\varepsilon_m}\right)(\nabla T \cdot E)E^* - \frac{1}{4} Re\,(\varepsilon_m\, \alpha\, |E|^2 \nabla T) \quad (13)$$

where $\alpha = \frac{\partial \varepsilon_m}{\varepsilon_m \partial T}$, and $\beta = \frac{\partial \sigma_m}{\sigma_m \partial T}$. The dot product $\nabla T \cdot E$ in (13) shows that only the component of the temperature gradient that's parallel to the applied field will contribute to the ET force in the Coulombic term. The first term dominates at low AC frequencies whereas the dielectric term has a relatively minor contribution to the generated force [22]. In our analysis we consider only the first part in Eq. (13) because relative variations in conductivity $(\Delta\sigma/\sigma)$ are usually much greater than relative variations in permittivity $(\Delta\varepsilon/\varepsilon)$ [22]. Figure 3 shows the direction of the applied electric and the temperature gradients for each isoDEP configuration. For microelectrode systems (Fig. 3A), the relevant temperature gradient is generated along the width of the microchannel as the electric field is applied in the same direction; in insulative-based devices (Fig. 3B) the relevant ET force is generated along the microchannel length in the direction of the applied field.

After the gradient of the temperature is calculated, the ET fluid body force is calculated with

$$f_{\mathrm{ET}} \approx \frac{M\, \nabla T\, \varepsilon\, E^2}{T} \quad (14)$$

where $T = 300$ K and M, a dimensionless factor that predicts the variation of the ET hydrodynamics body force with frequency, ≈ 6.6 when $\varepsilon\omega/\sigma \gg 1$, [22]. The quantity $\nabla T\, E^2$ is determined from the previous temperature gradient calculations (see sections 2.1 and 2.2). Finally, the electrothermal fluid velocity is calculated with

$$v_{\mathrm{ETH}} \approx \frac{f_{\mathrm{ET}}\, D_h^2}{32\, \mu} \quad (15)$$

where the hydraulic diameter is $D_{\mathrm{h}} = \frac{2\, r_{60}\, h}{r_{60} + h}$.

For Peer Review

A MATLAB program was used to calculate v_{DEP} and v_{ETH} for a range of system inputs. The suspending media conductivity (σ_m) was set to $10\ \mathrm{mS/m}$. The channel height and width were varied from two particle diameters to 200 particle diameters. Calculations were conducted for a 1 μm particle traveling at n = 1 particle diameters per second. It will be later shown that the results can be scaled for different particle sizes, DEP velocities, and media conductivity.

For the electrode-based device, the lid and base were composed of the same material and thickness (0.5 mm glass). However, the conductive wall was assumed to be silicon with a thickness of 5 mm and thermal conductivity of 150 W/(m·K).

For the insulative-based device, the base was assumed to be either 0.2, 0.5, or 1 mm thick glass or 0.5 mm silicon. The lid was either a glass coverslip (0.2 or 1 mm) or PDMS (1 mm). Glass and PDMS were considered to have the same thermal conductivity (1 W/(m·K)) in our model, while water has 0.6 W/(m·K). The thickness of both the base and lid were varied to investigate whether it significantly influences minimizing ET effects.

In addition, device parameters such as base material type (either silicon or glass) and lid material type were varied while fixing the microchannel heights, width ($w = 3h$), k^2 ($10^{14}\mathrm{V^2/m^3}$), and σ_m ($10\ \mathrm{mS/m}$) .

3. Results and Discussion

Figure 4 shows the relationship between k^2, particle size, the desired translation velocity (n), system length scale (δ), and applied voltage. For example, if a particle of a size 1 μm needs to translate at a speed of 10 μm/s under the applied DEP force, will requires k^2 value of $1.51 \times 10^{15}\mathrm{V^2/m^3}$ (Fig. 4A). Hence, by using a 20 $\mathrm{V_{rms}}$ source, the characteristic length scale of the device will be 84 μm (i.e., $L \approx 84$ μm for an insulative-based device or $r_{60} \approx 84$ μm for an electrode-based device).

For Peer Review

The impact of microchannel dimensions is shown in Figure 5. In general, microelectrode devices perform better than insulative devices for similar microchannel dimensions (Fig. 5A,B). Further, smaller microchannel dimensions (w and/or h < 10 particle diameters) will yield a more favorable performance, i.e., $v_{\mathrm{DEP}} \gg v_{\mathrm{ETH}}$. For insulative isoDEP devices (Fig. 5B,C) the electrode length scale may be relatively large (L > 100 μm) such that a small microchannel height becomes critically important. Coplanar electrodes could perhaps be integrated into the insulative-based device to reduce the distance between the electrodes and the origin (resulting in a smaller L) thus reducing unwanted ET flow. Increasing the lid thickness from 0.21 mm to 1 mm and base thickness from 0.5 mm to 1 mm in insulative isoDEP device decreased the $v_{\mathrm{ETH}}/v_{\mathrm{DEP}}$ ratio by approximately 3.7% and 7% respectively. In addition, the ratio of velocities $v_{\mathrm{ETH}}/v_{\mathrm{DEP}}$ was approximately 10 times less using a silicon substrate (Fig. 5C) compared to a glass substrate (Fig. 5B) for insulative isoDEP devices. Further, Figure 5 results are scalable. If particle speed is increased to n = 10, the the ratio of velocities should be multiplied by 10. If fluid conductivity is increased by 10, multiply the results by 10. If the particle size is increased by 10, multiply the results by 100.

Deep reactive ion etching (DRIE) of highly-doped silicon wafers to fabricate the electrode-based isoDEP device for microchannel heights greater than 20 μm can be challenging due to extended etching times and sidewall roughness generated during the etching process. However, some post-DRIE processing techniques suitable for ~10 μm etching depths, [40] might be used to smooth the scalloping effect. Electroplating of metals can be adapted for microchannel heights below 20 μm; however, achieving the desired vertically-straight and parallel microchannel sidewalls required for isoDEP field is challenging.

Insulative-based devices offer a low-cost fabrication alternative (soft lithography, hot embossing, etc.) but the distance between the electrodes are relatively larger compared to electrodes-based

For Peer Review

devices, hence requiring greater applied voltages. High gain amplifiers can be used but typically cannot reach high frequencies (limits typically less than 10 MHz) which is a disadvantage because some cells phenotypes, such as cytoplasm properties and lipid formation, can only be investigated at higher frequencies ~ 40-80 MHz [41].

Intuitively, the key design parameters to reduce ET flow is to facilitate heat transfer normal to the electric field direction and reduce heat transfer in the direction of the field. Moreover, heat transfer is connected to the volumetric heat flux (q''') which is constrained by the microchannel height and width. Hence, for a given k^2 ET flow reduction can be achieved by either having a material of a high thermal conduction (K) or decreasing the height (h), wall thickness (t_{wall}), width of the microchannel, and the base thickness. Further, $v_{\mathrm{ETH}}/v_{\mathrm{DEP}}$ is reduced for smaller particles moving at the same relative speed n. The use of smaller particles will decrease the size of the microchannel and electrode spacing thereby reducing volumetric heating.

4. Concluding Remarks

The premise of isoDEP device is to analyze cell subpopulations relying on DEP particle translation; however, due to unwanted electrokinetic motion, particularly ET flow, the operation of isoDEP can be compromised. In this study we developed scaling law analysis to obtain design rules to maximize DEP-induced particle motion relative to ET flow. Our results recommend that in order to reduce the effects of ET flow, for both electrode-based and insulative based devices, the height and width of the microchannel should be less than 10 particle diameters. In addition, designs that

For Peer Review

facilitate heat transfer normal to the field direction is benefitial; for example, using a silicon base enhances the performance of insulative-based isoDEP devices.

Acknowledgment

This material is based upon work supported by the National Science Foundation under Grant No. 1550509.

The authors have declared no conflict of interest.

5. References

[1] Li, M., Li, W., Zhang, J., Alici, G., Wen, W., *J. Phys. D* 2014, *47*, 063001.
[2] Martinez-Duarte, R., *Electrophoresis* 2012, *33*, 3110-3132.
[3] Voldman, J., *Annu. Rev. Biomed. Eng.* 2006, *8*, 425-454.
[4] Green, N. G., Morgan, H., *J. Phys. Chem. B* 1999, *103*, 41-50.
[5] Green, N. G., Morgan, H., Milner, J. J., *J. Biochem. Biophys. Methods* 1997, *35*, 89-102.
[6] Washizu, M., Suzuki, S., Kurosawa, O., Nishizaka, T., Shinohara, T., *IEEE Trans. Ind Appl.* 1994, *30*, 835-843.
[7] Washizu, M., Kurosawa, O., *IEEE Trans. Ind Appl.* 1990, *26*, 1165-1172.
[8] Asbury, C. L., Engh, G. v. d., *Biophys. J.* 1998, *74*, 1024-1030.
[9] Pethig, R., Huang, Y., Wang, X.-b., Burt, J. P. H., *J. Phys. D* 1992, *25*, 881-888.
[10] Chiou, P. Y., Ohta, A. T., Wu, M. C., *Nature* 2005, *436*, 370-372.
[11] Rashed, M. Z., Velasco, V., Williams, S. J., *J Indian I Sci* 2018, *98*, 85-101.
[12] Ramos, A., Morgan, H., Green, N. G., Castellanos, A., *J. Phys. D* 1998, *31*, 2338-2353.
[13] Pohl, H. A., *Dielectrophoresis : The Behavior of Neutral Matter in Nonuniform Electric Fields*, Cambridge University Press, Cambridge 1978.
[14] Allen, D. J., Accolla, R. P., Williams, S. J., *Electrophoresis* 2017, *38*, 1441-1449.
[15] Keim, K., Rashed, M. Z., Kilchenmann, S. C., Delattre, A., Gonçalves, A. F., Éry, P., Guiducci, C., *Electrophoresis* 2019.
[16] Huang, L., Zhao, P., Wang, W., *Lab Chip* 2018, *18*, 2359-2368.
[17] Tada, S., Omi, Y., Eguchi, M., *Biomicrofluidics* 2018, *12*, 044103.
[18] Tada, S., Eguchi, M., Okano, K., *Electrophoresis* 2019, *0*.
[19] Xuan, X., *Electrophoresis* 2008, *29*, 33-43.
[20] Sadeghi, A., Kazemi, Y., Saidi, M. H., *Nanosc. Microsc. Therm.* 2013, *17*, 173-193.

For Peer Review

[21] Green, N. G., Ramos, A., Gonzalez, A., Morgan, H., Castellanos, A., *Phys. Rev. E* 2002, *66*, 026305.
[22] Castellanos, A., Ramos, A., Gonzalez, A., Green, N. G., Morgan, H., *J. Phys. D* 2003, *36*, 2584.
[23] Horiuchi, K., Dutta, P., *Int. J. Heat Mass Transfer* 2004, *47*, 3085-3095.
[24] Lian, M., Islam, N., Wu, J., *IET Nanobiotechnol.* 2007, *1*, 36-43.
[25] Hawkins, B. G., Kirby, B. J., *Electrophoresis* 2010, *31*, 3622-3633.
[26] Kang, Y., Li, D., Kalams, S. A., Eid, J. E., *Biomed. Microdevices* 2008, *10*, 243-249.
[27] Qian, C., Huang, H., Chen, L., Li, X., Ge, Z., Chen, T., Yang, Z., Sun, L., *Int. J. Mol. Sci.* 2014, *15*, 18281-18309.
[28] Gray, D. S., Tan, J. L., Voldman, J., Chen, C. S., *Biosens. Bioelectron.* 2004, *19*, 1765-1774.
[29] Jaeger, M., Mueller, T., Schnelle, T., *J. Phys. D* 2006, *40*, 95.
[30] Tay, F. E., Yu, L., Pang, A. J., Iliescu, C., *Electrochim. Acta* 2007, *52*, 2862-2868.
[31] Ajdari, A., *Phys. Rev. E* 2000, *61*, R45.
[32] Green, N. G., Ramos, A., Gonzalez, A., Castellanos, A., Morgan, H., *J. Electrostatics* 2001, *53*, 71-87.
[33] White, F. M., Corfield, I., *Viscous Fluid Flow*, McGraw-Hill, New York 2006.
[34] Iliescu, C., Taylor, H., Avram, M., Miao, J., Franssila, S., *Biomicrofluidics* 2012, *6*, 16505-1650516.
[35] Pohl, H. A., *Dielectrophoresis: the behavior of neutral matter in nonuniform electric fields,* Cambridge University Press, Cambridge 1978.
[36] Burgreen, D., Nakache, F., *Phys. Chem. A* 1964, *68*, 1084-1091.
[37] Sunderland, J. E., Johnson, K. R., *Ashrae Trans.* 1964, *70*, 237-241.
[38] Hartnett, J. P., Kostic, M., *Advances In Heat Transfer*, Elsevier 1989, pp. 247-356.
[39] VanSant, J. H., Lawrence Livermore National Lab., CA (USA) 1983.
[40] Mohammed, Z. A. S., Olimpo, M., Poenar, D., Aditya, S., *Mater. Sci. Semicond. Proc.* 2017, *63*, 83-89.
[41] Hadady, H., Wong, J. J., Hiibel, S. R., Redelman, D., Geiger, E. J., *Electrophoresis* 2014, *35*, 3533-3540.

For Peer Review

Figure legend

Figure 1. (A) Illustration of the isoDEP microchannel geometry. Cross-sectional view of the (B) microelectrode device with electrodes serving as the walls and the (C) insulative device Variables for the analysis herein are labeled.

Figure 2. Schematic diagram of heat transfer resistance model for (A) the microelectrode-based device where the silicon is serving as electrodes separated by a gap and (B) insulative based device where the electrodes are a distance L from the origin.

Figure 3: The electric potential (solid red) and resultant electric field (dashed blue) for the (A) microelectrode and (B) insulative isoDEP systems. The primary direction of their respective electrothermal body force component is shown.

Figure 4: (A) Graph of the required gradient of field-squared, k^2, for the isoDEP system to have a particle translate at n particle diameters per second. (B) Contour plot of k^2 for a given system length scale and applied voltage.

Figure 5: Contour plots of the resulting $\nu_{\mathrm{ETH}}/\nu_{\mathrm{DEP}}$ for different isoDEP systems: (A) microelectrode, (B) insulator, and (C) insulator with silicon base. Results are for a 1 □m particle traveling at n = 1 diameters per second. Axis scaling is with respect to particle diameter. Note: These results are scalable for different particle speeds, particle sizes, and fluid conductivity; refer to manuscript for more information.

For Peer Review

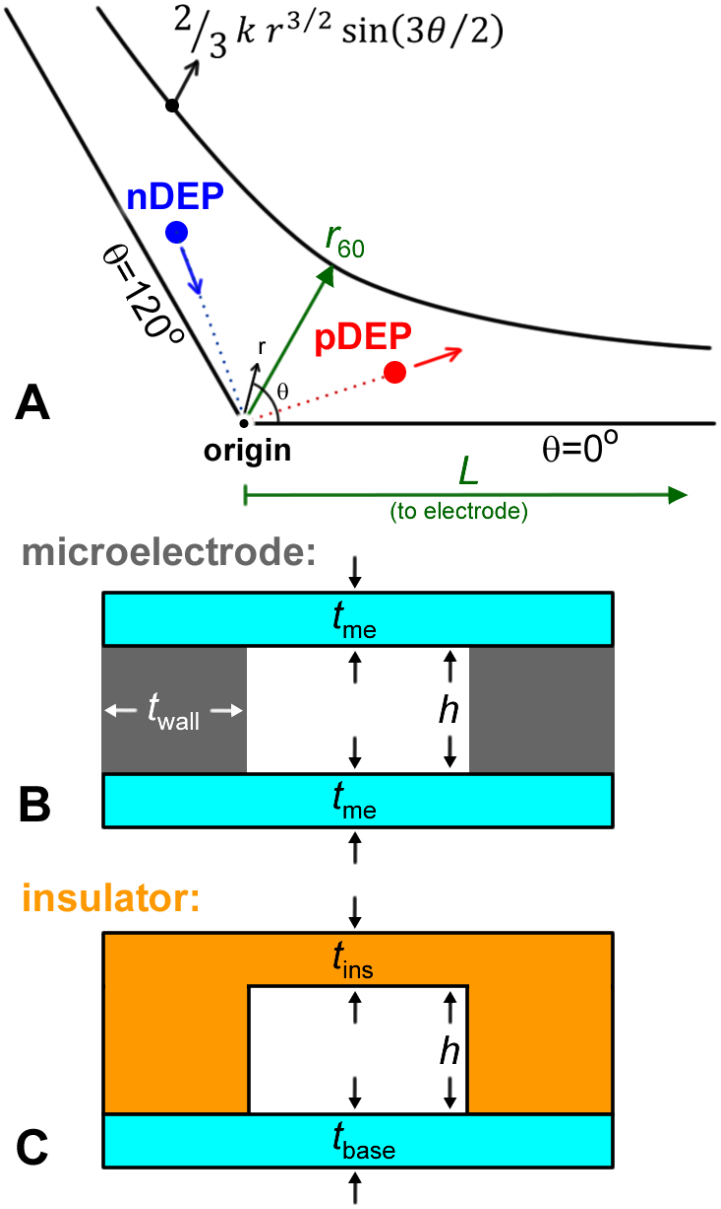

Figure 1. (A) Illustration of the isoDEP microchannel geometry. Cross-sectional view of the (B) microelectrode device with electrodes serving as the walls and the (C) insulative device Variables for the analysis herein are labeled.

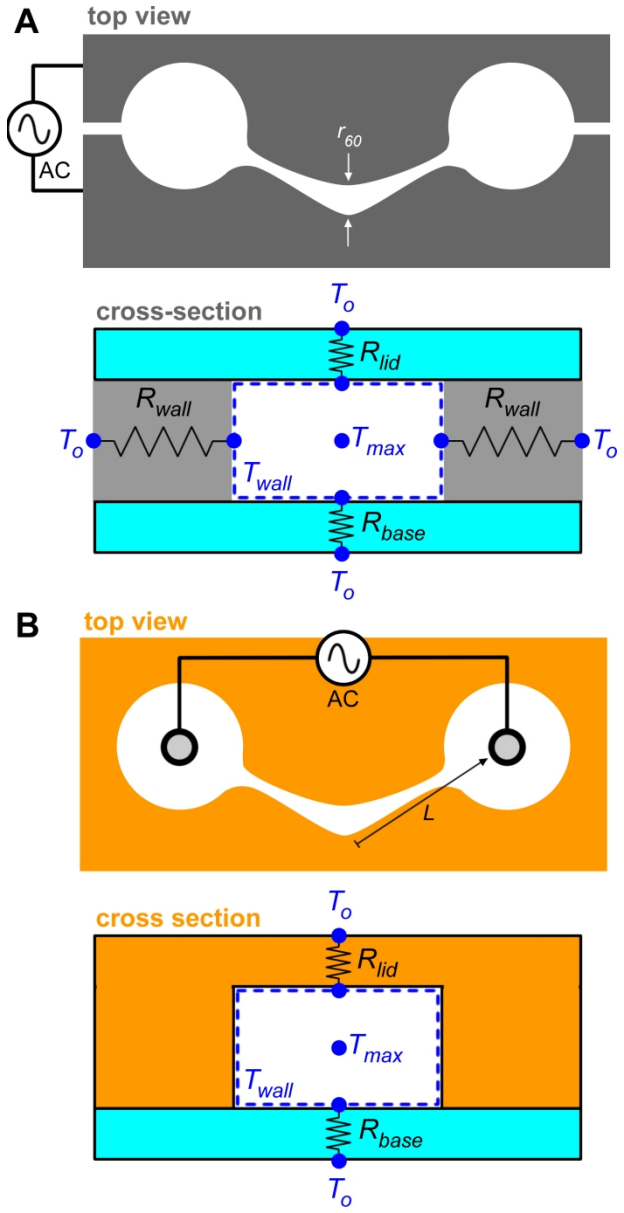

Figure 2. Schematic diagram of heat transfer resistance model for (A) the microelectrode-based device where the silicon is serving as electrodes separated by a gap and (B) insulative based device where the electrodes are a distance *L* from the origin.

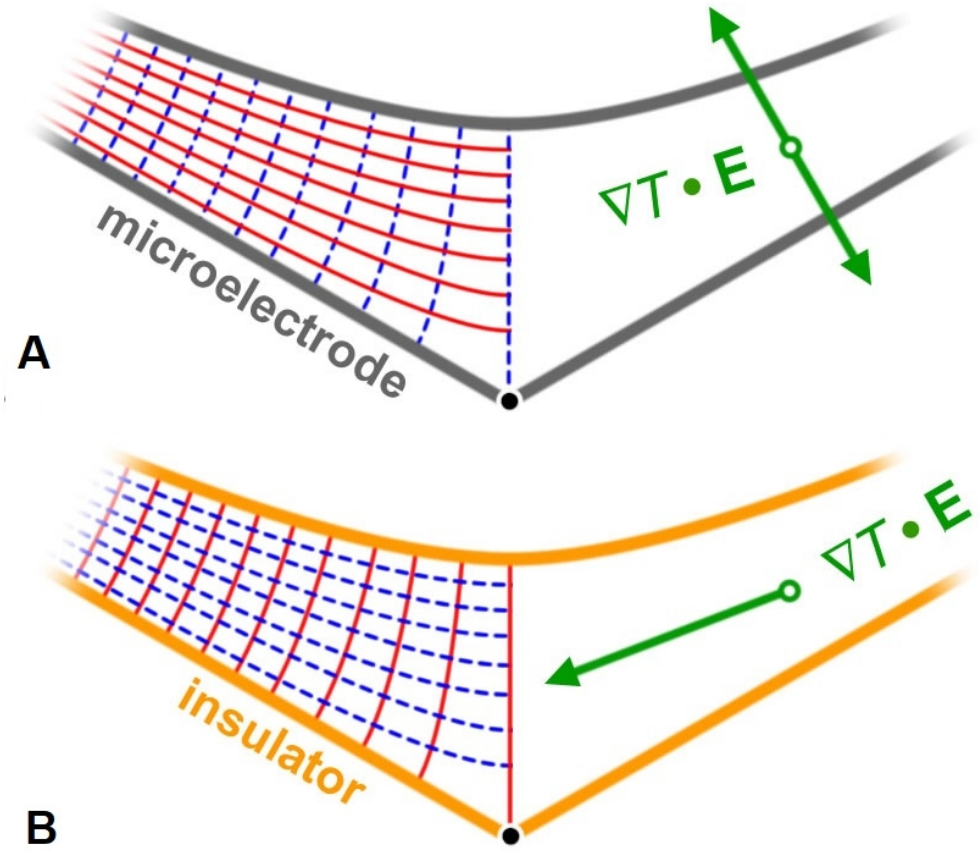

Figure 3. The electric potential (solid red) and resultant electric field (dashed blue) for the (a) microelectrode and (b) insulative isoDEP systems. The primary direction of their respective electrothermal body force component is shown.

86x74mm (240 x 240 DPI)

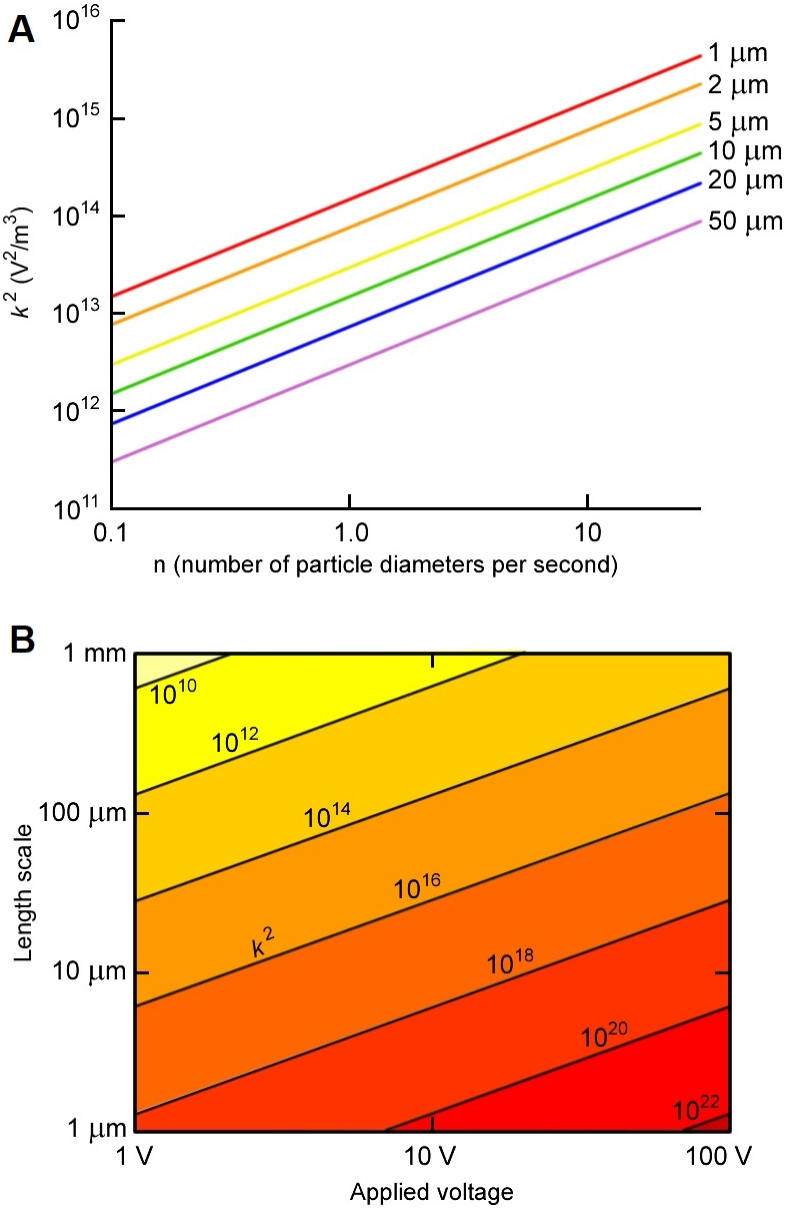

Figure 4. (a) Graph of the required gradient of field-squared, k^2 , for the isoDEP system to have a particle translate at n particle diameters per second. (b) Contour plot of k^2 for a given system length scale and applied voltage.

82x126mm (240 x 240 DPI)

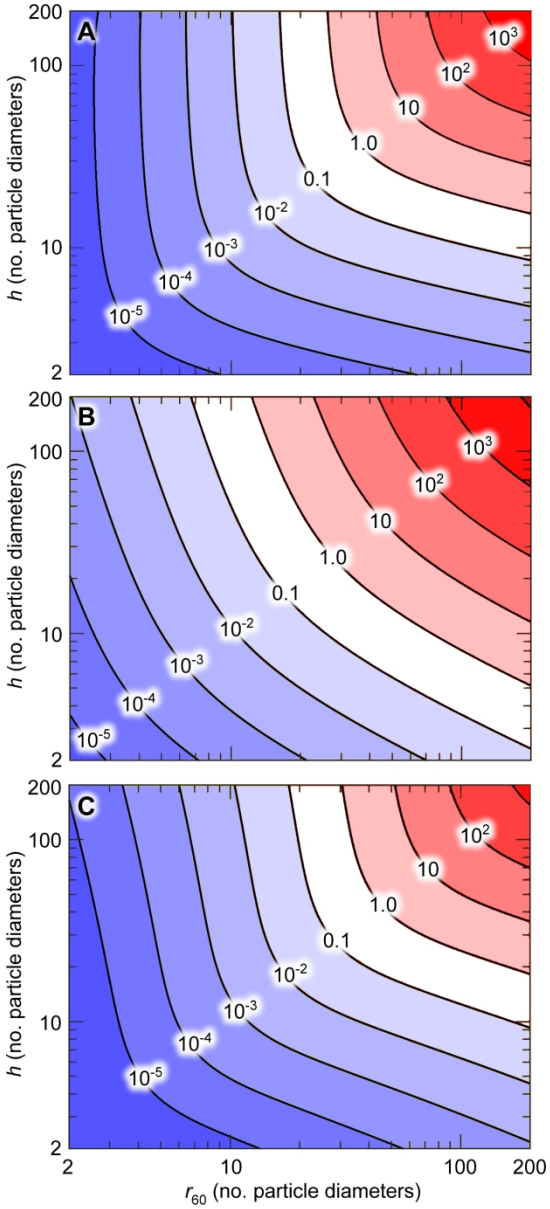

Figure 5. Contour plots of the resulting v_{ETH} / v_{DEP} for different isoDEP systems: (A) microelectrode, (B) insulator, and (C) insulator with silicon base. Results are for a 1 μm particle traveling at n= 1 diameters per second. Axis scaling is with respect to particle diameter. Note: These results are scalable for different particle speeds, particle sizes, and fluid conductivity; refer to manuscript for more information.

448x995mm (72 x 72 DPI)